Originally published as:

End-To-End Sensor Simulation for Spectral Band Selection and Optimization with Application to the Sentinel-2 Mission

Karl Segl,[1,*] Rudolf Richter,[2] Theres Küster[1] and Hermann Kaufmann,[1]

[1]Section 1.4 Remote Sensing, Helmholtz Center Potsdam, GFZ German Research Center for Geosciences, Telegrafenberg, 14473 Potsdam, Germany;

[2]DLR German Aerospace Center, Remote Sensing Data Center, D-82234 Wessling, Germany;

[*]Corresponding author: karl.segl@gfz-potsdam.de,

Tel.: +49 331 288-1193; Fax: +49 331 288-1192

Abstract: An end-to-end sensor simulation is a proper tool for the prediction of the sensor's performance over a range of conditions which cannot be easily measured. In this study (ESA-Contract: 19962/06/NL/EL) such a tool has been developed that enables the assessment of the optimum spectral resolution configuration of a sensor based on key applications. It employs the spectral molecular absorption and scattering properties of materials that are used for the identification and determination of the abundances of surface and atmospheric constituents and their interdependence on spatial resolution and signal-to-noise ratio (SNR) as a basis for the detailed design and consolidation of spectral bands for the future Sentinel-2 sensor. The developed tools allow the computation of synthetic Sentinel-2 spectra that form the frame for the subsequent twofold analysis of bands in atmospheric absorption and window regions. One part of the study comprises the assessment of optimal spatial and spectral resolution configurations for those bands used for atmospheric correction, optimized with regard to the retrieval of aerosols, water vapor and the detection of cirrus clouds. The second part of the study presents the optimization of thematic bands, mainly driven by the spectral characteristics of vegetation constituents and minerals. The investigation is performed for different wavelength ranges because most remote sensing applications require the use of specific band combinations rather than single bands. The results from the important "Red Edge" and the "Short Wave Infrared" domain are presented. The recommended optimum spectral design predominantly confirms the sensor parameters given by ESA. The system is capable of retrieving atmospheric and geo-biophysical parameters with enhanced quality compared to existing multispectral sensors. Minor spectral changes of single bands are discussed in the context of typical remote sensing applications, supplemented by the recommendation of a few new bands for the next generation of optical Sentinel sensors.

1. Introduction

An end-to-end simulation is a very useful tool for the design of any new Earth imaging system. Extensive sensitivity analyzes can be performed in order to estimate the influence of different instrumental or environmental parameters on scene characteristics. Hence, a careful simulation of reflectance, top-of-atmosphere (TOA) radiance and digital numbers (DNs) greatly facilitate the optimization of system requirements and the derivation of expected error budgets [1]-[5]. For years, band parameters of optical remote sensing systems were usually defined by the system engineers and not in particular driven by applications, respectively the spectral behavior of relevant surface cover types. The bands were placed predominately in the range of high transmission to minimize atmospheric effects and chosen as broad as possible to gain sufficient SNR values. New sensor technology allows the use of smaller band widths that bears the consequence to define optimal centering and width of each band on the basis of the optical transmission in combination with the spectral characteristics of the main surface cover types. We already conducted spectral optimizations in the frame of the spectral and panchromatic band definition of the German MOMS-02 sensor, resulting in a significantly improved retrieval of surface parameters [6],[7]. Initiated by the results of this experience over the years, we developed an end-to-end simulation tool for an application-driven optimization of the spectral band design of the new Sentinel-2 sensor representing the most prominent high spatial resolution multispectral remote sensing system for the next decade. The sensor system is being developed as part of the Global Monitoring for Environment and Security (GMES) program, jointly funded by the European Space Agency (ESA) and the European Commission (EC) [8]. The first of two satellites is scheduled for launch in 2013. When both satellites are operational and under cloud-free conditions, they will deliver data on land surfaces and coastal zones every five days. The system will provide enhanced continuity to the French SPOT and US Landsat missions. Based on user requirements, a preliminary set of channel center wavelengths and bandwidths was defined in 2005, and the objective of the ESA contract with GFZ/DLR was to consolidate these specifications [9]. The main investigations of the study were performed in 2006, and some updates from 2010/2011 are included as well [10]. All of these investigations were conducted in close cooperation with ESA engineers that provided the frame parameters for the simulation. The paper is organized as follows. The developed methodology is described in Section 2. Exemplary results are presented separately in Section 3 and 4. The first of the two sections describes the considerations concerning the spectral channels dealing with atmospheric correction and the retrieval of related atmospheric products. The second part studies optimum bands for selected land surface applications, such as the retrieval of chlorophyll a+b and liquid water content of plants and the differentiation of minerals. The main points are finally summarized in Section 5 including also some recommendations for the next generation of optical Sentinel sensors.

2. Methodology

Assessment of the optimum spectral resolution configuration requires the simulation of spectra using different Sentinel-2 sensor variations. For this purpose, an end-to-end sensor simulation was developed that employs the preliminary sensor parameters summarized in Table 1.

Table 1. Preliminary set of 13 spectral bands of Sentinel-2 (from MRD, SRD).

Spectral band	Center (λ) [nm]	Width ($\Delta\lambda$) [nm]	Lmin	Lref	Lmax	SNR@ Lmin	SNR@ Lref	SNR@ Lmax	GSD [m]
1	443	20	15.97	129.1	587.9	27.3	129	306.7	60
2	490	65	11.70	128.0	615.5	26.9	154	368.2	10
3	560	35	6.49	128.0	559.0	15.5	168	399.5	10
4	665	30	3.31	108.0	484.1	7.7	142	357.9	10
5	705	15	2.61	74.6	449.6	7.4	117	328.0	20
6	740	15	2.06	68.2	412.9	4.3	89	263.2	20
7	783	20	1.67	66.7	387.1	4.6	105	294.0	20
8	842	115	0.95	103.0	307.8	3.8	175	320.2	10
8a	865	20	0.95	52.4	307.8	1.9	72	219.2	20
9	945	20	0.51	8.8	172.5	10.8	114	614.08	60
10	1375	30	0.0	6.0	83.0		50		60
11	1610	90	0.4	4.0	66.8		100	540	20
12	2190	180	0.1	1.7	22.8		100	510	20

Note: λ is the center wavelength, $\Delta\lambda$ the spectral width of the spectral filter function, Lmin, Lref, and Lmax different radiance levels (W m^{-2} sr^{-1} μm^{-1}) with associated SNRs and GSD the spatial resolution.

The developed simulation approach consists of two parts - the sensor simulation and its inversion process (reflectance retrieval). Both are depicted in Figure 1.
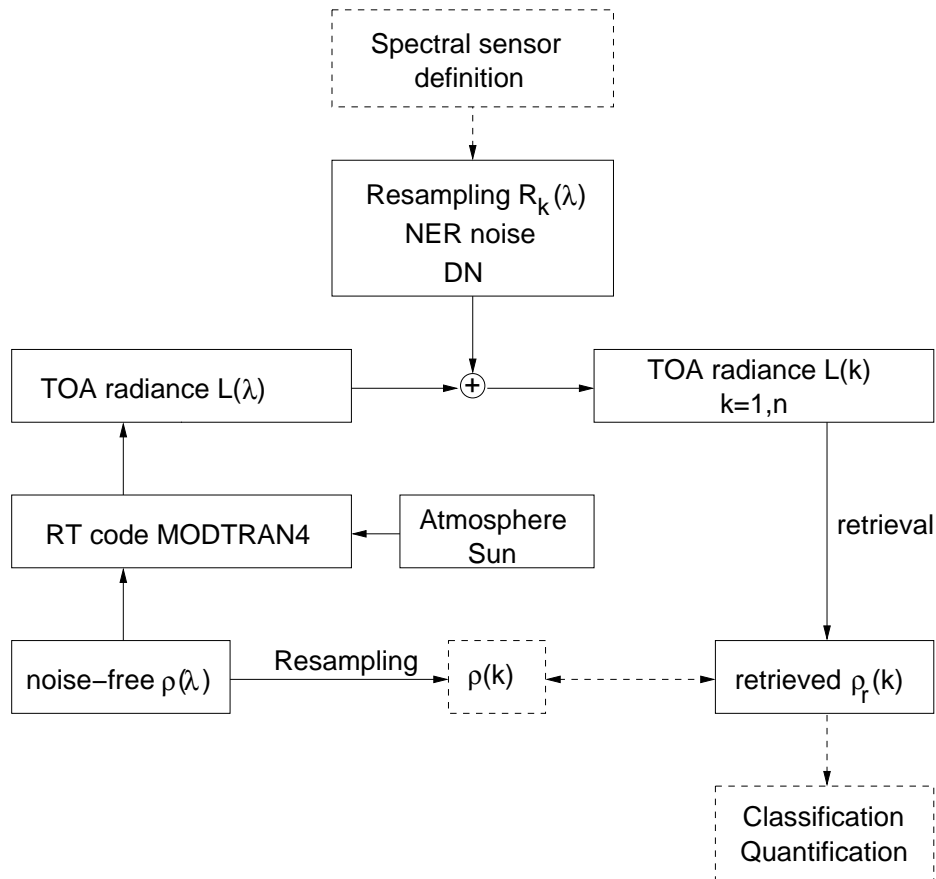

Figure 1. Schematic view of the simulation flow.

As input serve noise-free high spectral resolution reflectance data with a horizontal distribution of different surface components. The used spectra are predominately surface materials such as different vegetation, soil, mineral and man-made types, spectrally mixed spectra and spectrally flat targets (reflectance 0.1 and 0.2). In the first step the input image is transformed to a top-of-atmosphere (TOA) scene for specified atmospheric conditions and solar geometry using a radiative transfer (RT) model (MODTRAN4, [11],[12]). Then the high spectral resolution TOA radiance $L(\lambda)$ is resampled with the Sentinel-2 channel spectral response function $R_k(\lambda)$, where k indicates the band number. Each function is modeled by the following filter function that was provided by ESA engineer (1):

$$R_k(\lambda) = X_0 + X_s * e^{-\left| \frac{2(\lambda-\lambda_C)}{\alpha\Delta\lambda} \right|^{X_e}}$$

$$X_e = 6 \qquad \Delta\lambda = \text{FWHM}$$
$$X_0 = 0.0001 \qquad \lambda_c = \text{Center}$$
$$X_S = 0.8999 \qquad \alpha = 1.06299$$

(1)

The shape of this response function is more rectangular compared to the standard Gaussian function, allowing a more realistic description of filters used within multispectral sensors (Fig. 2).
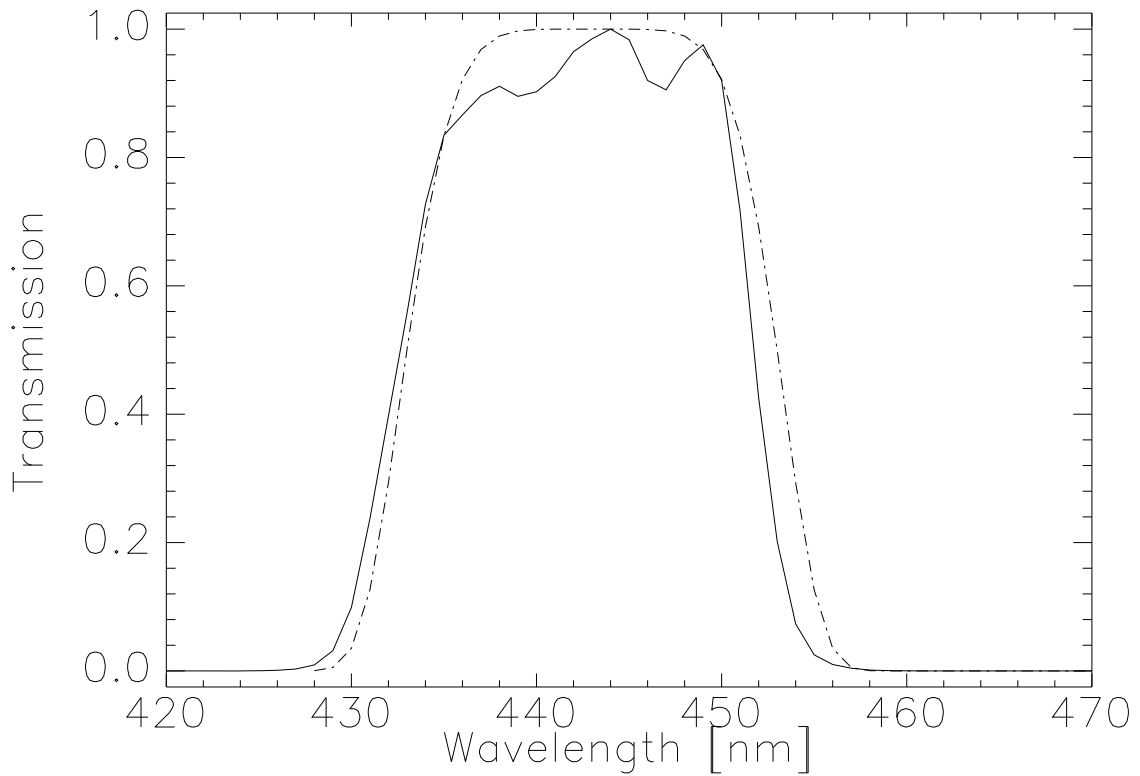

Figure 2. Band 1 – Spectral response function of Sentinel-2 (solid line) and modeled function (dashed line).

Noise is introduced as Gaussian noise in the simulation procedure that demands the calculation of noise equivalent radiance (NER = L/SNR(L)) values. The variable size of $\Delta\lambda$ is also considered, assuming dominating shot noise, i.e., the SNR depends on the square root of the radiance signal [13]. For example, if the bandwidth $\Delta\lambda$ decreases by the factor 4 with all other sensor parameters being the same, the NER is reduced by a factor 2. The resampled radiance data

5

are scaled between Lmax and Lmin to simulate the radiometric resolution of the sensor (12 bit). Then the inversion process starts by calibrating the sensor DN data (TOA radiance L(k)) followed by the atmospheric correction. Besides the surface reflectance $\rho_r(k)$ the aerosol optical thickness (AOT) at 550 nm and the water vapor column can be retrieved. In case of the optimization of atmospheric bands the obtained results can be directly compared to the known input parameters to assess the retrieval accuracy.

In contrast, the atmospheric parameters are kept constant in case of the optimization of bands for surface parameter retrieval assuming a standard atmosphere (e.g., mid-latitude summer atmosphere with water vapor column of 1.5 cm, rural aerosol model, visibility of 23 km, sea level, and a solar zenith angle of 40°). In addition, the processing scheme is supplemented by a spectral sensor definition tool and different quantification and classification tools. The sensor definition tool creates systematic variations of the spectral response functions altering the center wavelength λ_C and the width $\Delta\lambda$ within meaningful ranges defined by ESA engineers. In this way, up to more than 80,000 different sensor variations are generated depending on the number of simultaneously optimized bands. These spectral sensor designs are evaluated analyzing the retrieved reflectance spectra by quantification and classification tools. The accuracy achieved for the retrieval of representative vegetation and surface parameters serves as the quality measure for the optimization process.

3. Optimization of Atmospheric Correction Bands

The Earth's atmosphere scatters and absorbs solar radiation along the sun-earth-sensor path. Some effects can be accurately computed (Rayleigh scattering, absorption by uniformly mixed gases such as oxygen and carbon dioxide), others are difficult to assess (aerosol and water vapor) because they vary significantly in space and time. Sentinel-2 data will be influenced by ozone, aerosol, water vapor, and semi-transparent cirrus, and this influence is the subject of this section. Due to current technical constraints (recording capacity, downlink data rate), a high spatial resolution of 10 m can only be realized in some Sentinel-2 bands (B2: 490 nm, B3: 560 nm, B4: 665 nm, B8: 842 nm); others have a 20-m resolution (B5, B6, B7, B8a, B11, B12), and the remaining bands for aerosol, water vapor retrieval and cirrus detection are designed with a 60-m resolution. The reason for the reduced spatial resolution of some bands is that atmospheric conditions usually change slowly with distance, whereas surface features can exhibit high-spatial-frequency behavior, especially in urban environments. This contribution investigates the three channels intended for the retrieval of atmospheric parameters (aerosol, B1: 443 nm; water vapor, B9: 945 nm; cirrus, B10: 1375 nm). As the spatial resolution of these bands is fixed to 60 m, we only study the influence of shifts of the center wavelength and spectral bandwidth. Of course, the retrieval also requires other spectral bands that are already fixed for some reason (e.g., to capture relevant features of land surface signatures). Therefore, degrees of freedom only exist for the atmospheric bands, and we have to accept the spectral locations of the other bands as fixed.

3.1. Spectral Band Requirements for Aerosol Retrieval

Aerosol retrieval was performed with the dense dark vegetation (DDV) method [14]. The approach uses an empirical correlation of the surface reflectance between the visible and short-wave infrared (SWIR) bands. In the case of Sentinel-2, the bands B12 (2190 nm), B4 (665 nm),

B2 (490 nm) and B1 (443 nm) can principally be employed. The blue band B2 is similar to band 1 of Landsat TM / ETM+. Good results of the DDV method were obtained with Landsat imagery [15] employing the blue, red, and 2200-nm bands. Thus, the B1 is not absolutely necessary but could provide a useful additional spectral capability to determine the aerosol type (Angstrom coefficient). If B1 is included in the aerosol retrieval, the other bands (B4 at 10 m, B12 at 20 m) have to be spatially resampled to 60 m. In addition, the spectral correlation ρ (480 nm) = 0.5 ρ (red), with the standard coefficient 0.5 for channels in the 450-510-nm region (Landsat-5, Landsat-7 ETM+ band 1), has to be adapted to the new spectral range (B1: 430-455 nm). The necessary research to find a representative new correlation factor was outside the scope of this project, so the B2 and B4 were used.

Some aerosol retrieval experience with a 443-nm band exists for MERIS [16]. Here the atmospherically resistant vegetation index (ARVI, [17]) is employed to detect DDV pixels because MERIS has no SWIR bands. The DDV concept has been extended to include fewer dark pixels to obtain a higher percentage of pixels suitable for aerosol retrieval. Based on data from the POLDER instrument (6-km spatial resolution, [18]), 20 MERIS DDV models were defined for different seasons and geographic locations [16]. However, no comparable database exists for the 60-m spatial resolution of B1 of Sentinel-2. A certain advantage of an aerosol retrieval with the 20-m Sentinel-2 bands (B2, B4 resampled, B12: original) would be that more small-scale DDV pixels could be detected compared to a 60-m search, especially in urban areas. A separate investigation is needed to find the best trade-off for different situations.

In any case, the critical point is the assumption of the spectral band correlation factors (red to SWIR2 band and blue to red band). The simulated cases show that if the error in this correlation factor is greater than 10%, it will be the dominating error source for the aerosol retrieval, and radiometric calibration errors (smaller than 5% for Sentinel-2) will play only a minor role. Uncertainties in the aerosol scattering phase function and single scattering albedo can lead to a large over- or under-estimation of the aerosol optical thickness. However, smaller errors occur for the surface reflectance retrieval because the forward calculation of the TOA radiance and the reflectance retrieval use the same radiative transfer functions, causing a partially compensating effect [19].

Concerning the center wavelength and bandwidth of band B1: a small shift < 5 nm of the center wavelength and an increase of the 20-nm bandwidth to 30 nm is not critical for the aerosol retrieval because aerosol properties vary slowly with wavelength. Therefore, other arguments (e.g., derivation of coastal water constituents) can be used to decide on channel location and bandwidth.

3.2. Spectral Band Requirements for Water Vapor Retrieval

Several two- and three-channel water vapor retrieval methods have been published: the narrow/wide band ratio (N/W, [20]), continuum interpolated band ratio (CIBR, [21]), and atmospheric precorrected differential absorption technique (APDA, [22]). In this study, we use the APDA approach. Figure 3 presents a typical atmospheric transmittance curve in the 0.5- to 1.1-µm spectrum and a canopy reflectance spectrum. The grey bars indicate configurations for water vapor bands.
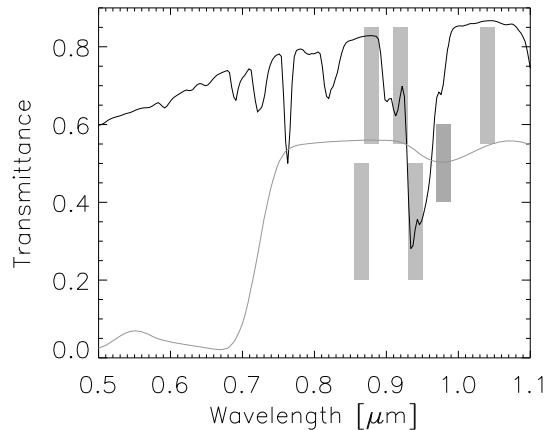
Figure 3. Atmospheric transmittance (top), canopy reflectance (bottom), and water vapor band configurations.

With three channels (one in the 940-nm absorption, two on the left and right shoulder window regions), it is easier to perform a linear interpolation across the absorption region to estimate the depth of absorption. However, a linear interpolation is not always the best choice: vegetated surfaces show non-linear reflectance behavior in the 940- to 990-nm region (plant water), as do soils with iron content. Additionally, a second window channel (in the 1010–1040-nm region) is not favored because of the limitation of 13 bands. The alternative would be to drop the 443-nm blue band, which was not considered justifiable. Thus, a two-channel solution remained, with a possibility to shift the 940-nm band to 920 nm to reduce the influence of plant water on the reflectance estimate. In this case, a drawback would be a higher spectral accuracy requirement, because of the stronger slope of the absorption. Other possibilities (a shift of the 865-nm channel B8a to 875–880 nm, an increase of the bandwidth of B8a from 20 nm to 30 nm) were also investigated to reduce the spectral distance and thus the uncertainty in the reflectance estimate for the absorption channel. However, these options did not significantly improve the 5–10% accuracy of the 865-/945-nm water vapor retrievals for the test scenes. Therefore, the final choice was B9 at 945 nm (bandwidth 20 nm), and the choice for B8a (865 nm, bandwidth 20 nm) was already dictated by spectral reflectance considerations for land surfaces.

One question is related to the influence of the assumed atmospheric temperature/humidity altitude profile. The recommendation is to employ at least a summer and a winter profile, i.e., summer scenes should be processed with look-up tables (LUTs) based on a summer profile and winter scenes with winter LUTs. Relative RMS errors for water vapor retrieval increase by 6% if winter scenes are processed with summer LUTs and vice versa. A coarse criterion for the summer/winter decision could be based on monthly averaged land surface temperature (LST) maps from MODIS, which are available on a global scale, e.g., winter conditions could be assumed if LST < 5°C.

3.3. Spectral Band Requirements for Cirrus Cloud Detection

Cirrus clouds normally occur in the upper troposphere. Thin semi-transparent cirrus clouds over land are difficult to detect in atmospheric window regions. A narrow spectral band at

8

1.38 µm was proposed [21] for cirrus detection and subsequently included in MODIS, and it is now being used operationally in the MODIS processing chain [24]. The 1.38-µm region strongly absorbs solar radiation due to water vapor. This trace gas concentrates in the lower 5 km of the atmosphere and completely absorbs ground-reflected radiation. Because cirrus clouds occur at higher altitudes, they scatter solar radiation, which can be recorded by a spaceborne instrument without a disturbing ground signal.

Our study uses radiative transfer calculations with the MODTRAN4 code to investigate the sensitivity of the channel position and bandwidth for band B10. The calculations are performed for a nadir view, ground at sea level, a rural aerosol with a visibility of 23 km, a solar zenith angle of 40°, and low to medium water vapor columns (WV = 0.4, 1, 3 cm). A spectrally constant surface reflectance of 0.3 is selected, which is typical for vegetation and soils in the 1.3- to 1.5-µm region. TOA radiance results are calculated for a 1-nm spectral grid and resampled to three synthetic sensor configurations with bandwidths of 10, 20, and 30 nm using a channel sampling distance of 3 nm after resampling. Figure 4 presents selected results, where the WV = 3 cm case is omitted.
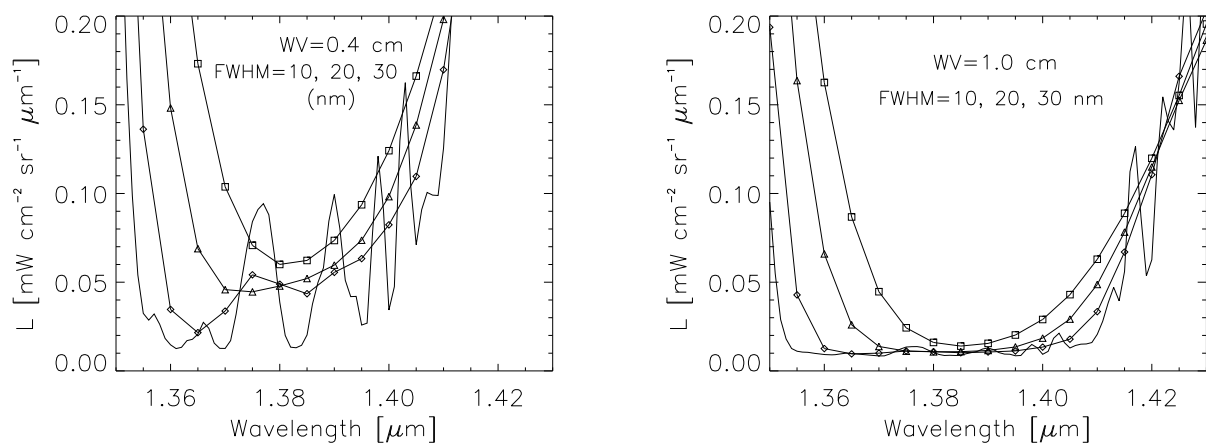

Figure 4. TOA radiance as a function of channel position and bandwidth (1, 10, 20, 30 nm: no symbol, diamond, triangle, square, respectively).

The high frequency curve for the low water vapor (WV = 0.4 cm, Fig. 3, left) indicates the highest spectral resolution (1-nm grid and Gaussian bandwidth). The other three curves contain the resampled results with larger bandwidths. For the lowest water vapor (0.4 cm) and the 1-nm bandwidth, ground reflected radiation can be observed in some parts of the 1.37 to 1.39-µm region, where the atmospheric transmittance is slightly higher and details of the narrow absorption band structure due to water vapor can be observed. These details are smoothed with an increase in spectral bandwidth. Fig. 3 (right) demonstrates how much the TOA radiance decreases even with a moderate increase in the water vapor column (from 0.4 cm to 1 cm). The best position for a channel with 30-nm bandwidth is in the 1.38- to 1.39-µm region (square symbol). For a channel with a 20-nm bandwidth, the spectrum of 1.370- to 1.395 µm is suitable because no ground-reflected radiation can be detected. The current ESA decision for band B10 is

a center wavelength of 1.375 μm and a bandwidth of 30 nm, but a center wavelength at 1.380 μm would perform somewhat better, reducing the TOA radiance signal by about 15% (at WV=0.4 cm) and 34% (at WV=1 cm), compare Fig. 3.

3.4. Ozone and Methane Influence

The ozone column cannot be retrieved with the available Sentinel-2 bands. Although the ozone concentration does not vary as rapidly in space and time as aerosol and water vapor do, it has some influence on the surface reflectance calculations for bands B1 to B5; see Figure 5.
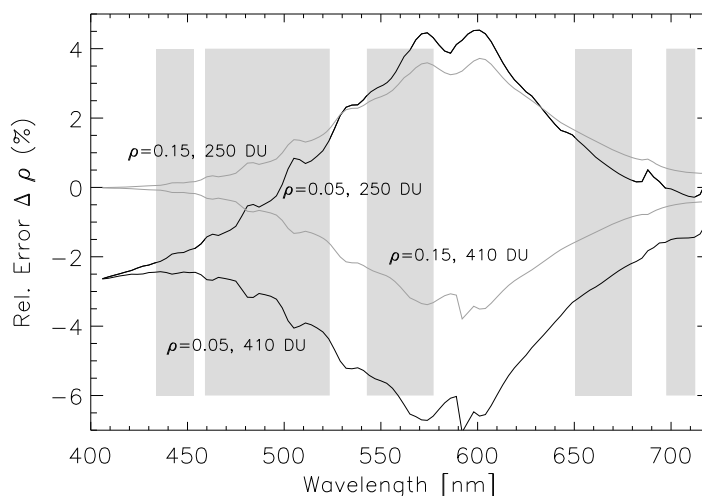

Figure 5. Surface reflectance error as a function of ozone column for ρ = 0.05 and 0.15, assuming an atmosphere with 330 DU (shaded areas: Sentinel-2 bands B1 to B5).

Figure 5 presents the relative surface reflectance errors for ρ = 0.05 (black curves) and 0.15 (grey curves) for ozone columns of 250 DU and 410 DU if the retrieval is performed with the assumption of 330 DU. The interval 250 – 410 DU covers a representative range of moderate ozone variations excluding extreme values. The highest sensitivity exists in the green band, B3, where relative errors of up to about 6% occur. The two cases with ρ = 0.05 and 0.15 are typical for vegetation, water, and soil targets. To account for varying ozone levels, it is recommended to use ozone measurements from other sources (e.g., GOME-2) from the same day and location. An average, constant ozone value per Sentinel-2 scene would improve the accuracy of the surface reflectance retrieval. A discrete set of ozone-dependent LUTs can be calculated (e.g., to cover the 250- to 410-DU range with an increment of 40 DU), and the LUT nearest to the measured value will be selected. Of course, on a global scale, the dynamic range of ozone concentrations is larger than the selected 250- to 410-DU example interval, and a trade-off between typical representative values and the affordable number of LUTs is necessary.

10

Atmospheric methane has a very small absorption influence around 1.65 μm and cannot be retrieved. The simulations are based on a climatological average methane concentration of 2 ppmv. The transmittance influence on the relatively broad B11 is smaller than 0.5%.

4. Optimization of Bands for Surface Parameter Retrieval

This section deals with defining the optimum width and centering of bands from the Red Edge domain (bands B4, B5, B6, B7, B8, and B8a) and the Short Wave Infrared domain (bands B11 and B12). Selected results from the spectral consolidation study [9] are presented.

4.1 Spectral Sensitivity Analysis for the Red-Edge Bands

For vegetation, the Red Edge characteristic [25] is the most prominent feature in the VNIR wavelength range. Vital leaves and canopies are characterized by high reflectance values (mesophyll) in the NIR, and the steep fall-off towards the visible range is due to strong pigment absorptions, such as chlorophyll-a in the 630- to 690-nm region. This area has been selected as the main focus of many investigations due to its unique spectral characteristics. Investigations based on laboratory and field spectra have shown that the position and shape of the Red Edge contain information about the biomass, chlorophyll content, physiological stress of vegetation and Leaf Area Index (LAI) [25]-[29]. This region is also strongly influenced by the spectral characteristics of transition elements in soils and rocks. The most prominent one is iron in its bi- and trivalent states, which display strong charge transfer bands (UV), crystal field absorptions (VIS) and conduction bands (NIR). The majority of Fe-bearing minerals show broad absorption wings that are unstable in their wavelength ranges and overlap each other. Consequently, minerals containing Fe^{2+} or Fe^{3+} are not the main focus of these investigations, but the detectability of these features and their influence on the spectral behavior of vegetation targets are taken into account.

A spectral library is required that serves as an input for the sensor optimization tool. Each reflectance spectrum of the library is copied into 100 image pixels to obtain representative noisy variations. These image spectra are transformed according to different sensor definitions and are evaluated in the subsequent data analysis to select the best sensor configuration. Hence, these sample spectra have a significant impact on the final optimization result and must be selected carefully. The acquisition of biochemical leaf parameters is a difficult task, so many investigations apply leaf transfer models to simulate reflectance characteristics based on these parameters. For this investigation the PROSAIL model [30] was used to generate top-of-canopy reflectance combining the leaf optical properties model PROSPECT [31],[32] and the canopy model SAIL [33]. Different spectra with a spectral resolution of 1 nm were generated varying the chlorophyll a+b content from 5.0 - 100.0 μg/cm2 with a step size of 5.0 μg/cm2 and the LAI between 0.5 – 4.0. The LAI controls the density of the canopy within the SAIL model and therefore the mixture of the vegetation signal with the soil background. Such spectral mixtures represent the most important limitation for the estimation of biochemical leaf parameters. Consequently, this issue is also addressed in the simulation. Two spectral libraries were generated including typical spectra of dense canopies in Lib1 (LAI = 3,4) and of less dense canopies in Lib2 (LAI = 0.5,1,2). Three iron-based mineral spectra (goethite and hematite) from the USGS library were selected as background spectra showing strong variations in the Red Edge

11

region and, thus, represent a major challenge for the retrieval of vegetation parameters in remote sensing applications.

The optimization process is based on the accuracy of the chlorophyll retrieval achieved in the quantification process. For this purpose, the Red Edge reflectance characteristics must be modeled. Sentinel-2 operates six bands in this wavelength region. One is located in the absorption of chlorophyll-a (B4), two are placed directly along the Red Edge (B5 and B6) and three (B7, B8, and B8a) are placed within the so-called Infrared area. The high number of bands enables the application of more precise models compared to most prominent vegetation indices, such as the inverted-Gaussian Reflectance Model (IGRM) [34].
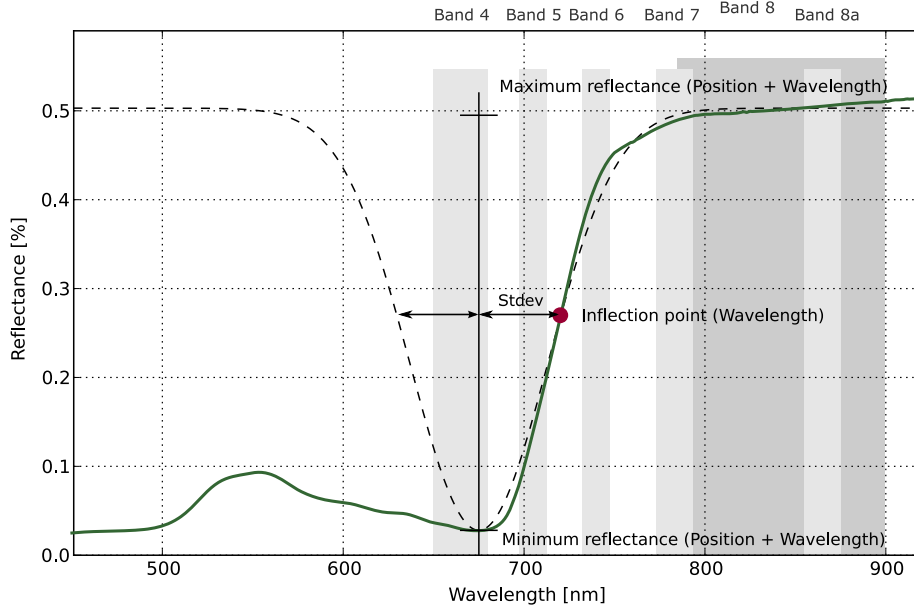

Figure 6. Inverted-Gaussian Reflectance Model (IGRM).

In this model, the Red Edge reflectance $\rho(\lambda)$ is a function of the maximum reflectance (ρ_{Max}) in the NIR range, the minimum reflectance (ρ_{Min}) and its wavelength (λ_{Min}), the standard deviation σ and the wavelength λ (Fig. 6):

$$\rho(\lambda) = \rho_{Max} - (\rho_{Max} - \rho_{Min}) * e^{\dfrac{-(\lambda - \lambda_{Min})^2}{2\sigma^2}} \tag{2}$$

Standard numerical procedures are employed to estimate the best fit between the model and the reflectance data according to the least squares criterion. The estimated parameters describe the shape of a vegetation spectrum and can be used for parameter retrieval. Thereby a fifth parameter – the wavelength of the inflection point ($\lambda_P = \lambda_{Min} + \sigma$) of the reflectance edge slope – is of specific interest. This parameter provides an additional measure of the position of the Red Edge reflectance of vegetation and is less affected by variations in soil/rock background compared to commonly used vegetation indices such as NDVI or SAVI. Studies have demonstrated the potential of this parameter for the retrieval of vegetation parameters using

12

linear and non-linear regression models [35], [29]. As an example, Figure 7 depicts the excellent correlation between leaf chlorophyll a+b and the inflection point (R^2 = 0.98, RMS = ± 3.8 µg/cm^2) using a second order polygon. The correlation plot is calculated from the Lib1 library using all bands from the Red Edge region.

The plot shows:
$$y = 0.1083\, x^2 - 150.3508\, x + 52204.4056$$
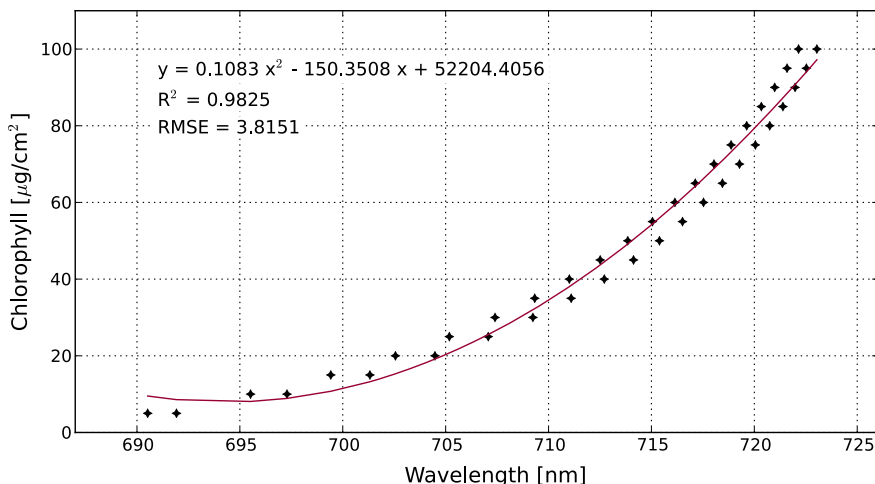$$R^2 = 0.9825$$
$$RMSE = 3.8151$$

Figure 7. Correlation plot depicting the dependency between chlorophyll a+b content and wavelength of the inflection point (IGRM).

A minimum of four bands is required to calculate the position of the inflection points. Hence, three different band settings were investigated using different NIR bands (B7, B8, and B8a). Up to more than 80,000 different spectral sensor configurations were defined by varying center and width of each band within the predefined ranges (Table 2) using a step size of 5 nm.

Table 2. Parameter ranges for band centers (λC) and band width ($\Delta\lambda$)

	Band 4	Band 5	Band 6	Band 7	Band 8	Band 8a
Left: $\lambda_C - \Delta\lambda$ [nm] Right: $\lambda_C + \Delta\lambda$ [nm]	630 690	700 740	720 750	770 810	775 890	840 890
Min: $\Delta\lambda_{Min}$ [nm] Max: $\Delta\lambda_{Max}$ [nm]	30 50	15 40	15 30	20 40	115 115	20 50

The best configurations for each library and band setting and their retrieval accuracy (RMS) are listed in Table 3.

Table 3. Results of optimized chlorophyll retrieval using the IGRM.

LAI	Bands	Sensors	RMS ESA [µg/cm²]	RMS Best [µg/cm²]	Band 4 λ / Δλ	Band 5 λ / Δλ	Band 6 λ / Δλ	Band 7/8/8a λ / Δλ
4.0/3.0 (Lib1)	4 5 6 7	43056	17.1	5.4	675/30	710/20	735/30	785/30
	4 5 6 8	3312	18.8	5.6	675/30	710/20	735/30	832/115
	4 5 6 8a	82800	19.2	5.5	675/30	710/20	735/30	860/40
2.0/1.0/0.5 (Lib2)	4 5 6 7	43056	18.1	10.8	675/30	710/20	740/20	790/20
	4 5 6 8	3312	18.4	10.9	675/30	710/20	740/20	832/115
	4 5 6 8a	82800	18.8	10.9	675/30	710/20	740/20	860/25

The results show that a re-definition of bands B4 through B7 delivers more accurate results compared to the preliminary definition by ESA. The achieved RMS for spectra from the Lib1 spectral library is only slightly degraded by the use of only 4 bands compared to hyperspectral data (see Fig. 7). In addition the retrieval algorithm could successfully be applied to the Lib2 spectral library showing that the IGRM is less affected by the soil background. A further spectral sensitivity analysis was carried out analyzing varying positions and widths of each single band. As a result only B4 is significantly sensitive. Table 4 depicts the results for chlorophyll retrieval using fixed optimized bands B5 through B7 and only variations of B4.

Table 4. Spectral sensitivity analysis of band 4

RMS Chlorophyll [µg/cm2]		FWHM [nm]						
		15	20	25	30	35	40	50
Center [nm]	**660**	27.1	27.4	27.3	27.2	27.2	27.1	27.2
	665	19.9	19.8	19.8	19.9	19.7	19.9	20.7
	670	9.1	8.7	8.8	8.8	8.8	8.9	9.2
	675	5.7	5.5	5.5	5.4	5.5	5.5	5.7
	680	4.9	4.8	4.8	4.7	4.9	4.8	4.9
	685	4.9	4.9	4.8	4.8	4.9	4.9	4.9
	690	5.2	5.2	5.2	5.2	5.2	5.1	5.1
	695	6.0	5.8	5.8	5.7	5.7	5.6	5.7
	700	7.1	6.9	6.8	6.7	6.5	6.5	6.4
	705	10.3	10.2	10.7	10.5	10.6	10.9	11.3

The analysis demonstrates that a shift of B4 towards shorter wavelengths deteriorates the accuracy of the results. A shift of the center to 670 nm represents the absolute lowest boundary technically possible. The optimum band is located between 680 and 685 nm, representing the position of the maximum chlorophyll absorption. This result becomes even more evident when examining the used Gaussian model. All bands should be centered at the Red Edge part of the Gaussian function where both curves show a perfect overlap (Fig. 5). The position of B4 is of high importance and should be close to the inverted maximum of the Gaussian function.

4.2. Spectral Sensitivity Analysis for the SWIR Bands

Within the SWIR range, there are two atmospheric windows centered at 1.65 μm (B11) and 2.2 μm (B12) that are characteristic for water content in plants. Additionally, they are influenced by vegetation structure (e.g., lignin/cellulose) and numerous minerals, especially phyllosilicates such as clays and micas. The 1.65-μm window is used to assess water content in plants and to differentiate between clouds, snow and ice. It is also characterized by the highest reflectance of minerals and rocks within the entire VNIR-SWIR range. To some extent, the 2.2-μm region is also sensitive to water stress phenomena, although it tends towards saturation at higher water content values. Band 12 is suitable to detect and quantify dry vegetation (structure) at 2.1 microns, although its signal is contaminated by CO_2 absorption. It also allows discriminating minerals in soils and rocks containing bound or un-bound water in the 2.2-μm (containing Al-OH) to 2.3-μm (bearing Mg-OH/C-O) wavelength range. Both bands are also usable for accurate aerosol retrieval, although the 1.6-μm region is preferred. Hence, the retrieval of plant liquid water and the discrimination of the Al-OH minerals are key applications for optimizing the SWIR bands.

4.2.1. Global Moisture Vegetation Index

The Global Vegetation Moisture Index (GVMI) is a simple numerical indicator that allows the retrieval of vegetation water content [36]. The GVMI is calculated using a NIR and a SWIR band:

$$GVMI = \frac{(NIR + 0.1) - (SWIR + 0.02)}{(NIR + 0.1) + (SWIR + 0.02)} \qquad (3)$$

This index minimizes perturbing geophysical and atmospheric effects. NIR and SWIR stand for the spectral reflectance measurements acquired in the near-infrared and shortwave infrared regions, respectively. According to its mathematical definition, the GVMI of an area covered by a dense and vital vegetation canopy tends to show positive values (e.g., 0.3 to 0.8). Other targets, such as soil or rocks, generate smaller or even negative values. B11 (SWIR) of Sentinel-2 is sensitive to changes in plant liquid water, whereas B8 (NIR) is only marginally affected.

The input of the band optimization process serves a spectral library generated again by the PROSAIL model [29]. The leaf equivalent water thickness is varied between 100 and 500 μm in steps of 10 μm and the LAI between 3 and 4. All other parameters are set to representative mean values. Due to SNR requirements at low energy levels in this wavelength region, B11 is varied within the edges between 1.5 μm and 1.75 μm, where no significant atmospheric

absorption takes place apart from slight water bands. The GVMI is calculated for all spectra and correlated with the plant liquid water using a second-order polynomial regression model. The results represented by the RMS error are depicted in Table 5, recommending a band around 1600 nm with a width of about 100 nm for this type of application.

Table 5. Spectral sensitivity analysis of band 11 (GVMI).

RMS water thickness [µm]		FWHM [nm]					
		50	75	100	125	150	175
Center [nm]	1580	31.9	31.8	31.9	32.0	32.2	32.3
	1600	32.0	31.9	31.8	31.9	32.1	32.3
	1620	32.2	32.1	32.1	32.2	32.3	32.5
	1640	32.5	32.5	32.6	32.7	32.7	32.8
	1660	33.2	33.2	33.2	33.3	33.2	33.2
	1680	34.3	34.1	34.1	33.9	33.7	33.5

4.2.2. Mineral Classification

An optimization of the SWIR bands B11 and B12 using mineral spectra is somewhat difficult because two bands are actually insufficient to conduct a meaningful classification. Therefore, the discrimination has been reduced to the separation between characteristic minerals of the Al-OH group (e.g., kaolinite, muscovite, pyrophylite) and those of the Mg-OH/C-O group (e.g., epidote, serpentinite and calcite) showing characteristic spectral absorption features at 2200 nm and 2320–2340 nm, respectively. Different sample spectra were collected from U.S. Geological Survey (USGS) and Jet Propulsion Laboratory (JPL) spectral libraries for this purpose.

Distinctive information is stored foremost in B12, and the variation of this band affects the optimization much more strongly than does variation of B11. Nevertheless, this band is necessary to highlight the absorption characteristics. The Spectral Angle Mapper (SAM) algorithm represents an appropriate classifier for this task. It is used to discriminate between the two mineral groups. B12 is varied within the entire window, avoiding CO_2 absorption at the shorter wavelength edge (2.09 µm) and CH_4 at the longer wavelength edge. Unfortunately, due to detector sensitivity at the right edge, there is a strict cut-off at 2.28 µm. Calculations are carried out by gradually decreasing the bandwidth to analyze the detectability of minerals, taking into account the trade-off between bandwidth and SNR. The accuracy of the achieved classification result is defined by the mean omission error calculated from the confusion matrix.

The results from different centerings and widths of B12 in combination with the preliminary B11 (1610/90 nm) are presented in Table 6. It shows a clear minimum at 2190 nm and 50 nm width. However, the SNR already seems to be too low for other applications employing this band. Especially, the detection of coniferous trees (DDV) for aerosol retrieval is

16

critical, requiring a minimum width of 100 nm. If higher SNR is still required, the band should be centered at 2190 nm.

Table 6. Spectral sensitivity analysis of band 12 (SAM)

Classification Error [%]		FWHM [nm]							
		30	40	50	60	80	100	140	180
Center [nm]	2150	36.3	35.2	34.3	35.1	38.6	37.0	32.5	30.9
	2160	30.1	29.4	38.4	38.7	39.3	35.8	32.9	35.1
	2170	29.7	29.6	28.5	36.4	34.1	33.6	33.2	36.2
	2180	27.7	24.7	24.9	24.5	30.3	28.5	31.0	36.7
	2190	18.4	16.1	15.0	15.1	17.6	20.6	29.7	38.4
	2200	21.7	21.5	20.8	20.6	21.4	19.9	34.9	38.4
	2210	20.2	21.0	23.4	24.7	23.0	23.8	38.6	41.2
	2220	35.7	28.3	29.3	29.9	29.7	34.4	38.0	38.3

4. Conclusion and Outlook

The 13 channel Sentinel-2 MSI is a major improvement over existing high spatial resolution multispectral satellite instruments. This set of bands covers the mission needs in terms of land use mapping, retrieval of geo-biophysical parameters and change detection. It includes three bands at a reduced spatial resolution of 60 m dedicated to atmospheric correction. Because many satellite scenes are contaminated by cirrus clouds, a cirrus band near 1375 nm is indispensable to detect and possibly correct for the effect of thin cirrus clouds. A water vapor band in the 940-nm region is also a new feature for MSI instruments that not only allows the derivation of a water vapor map, but accurate values will also reduce the residual influence of water vapor on the retrieval of surface reflectance in some channels (e.g., 1600 nm, 2200 nm).

For the aerosol retrieval, a second blue band (443 nm) is introduced in addition to the existing 490-nm band. This is certainly a viable option, especially if the 443-nm band is also useful for other purposes (e.g., coastal water). Another investigated option was to abandon the 443-nm band, shift the 490-nm channel to 475 nm and introduce a channel around 1020 nm for an improved three-channel water vapor retrieval. This makes sense if the retrieval of water vapor has the highest priority, but it requires a trade-off with other requirements. Another recommendation concerned the use of LUTs for summer and winter conditions based on a temperature threshold from monthly averaged global LST maps of MODIS. A further suggestion is the use of ozone measurements from other sources and ozone-dependent LUTs to improve the surface reflectance retrieval in the first five Sentinel-2 bands.

The availability of several bands within the Red-Edge domain significantly improves the characterization of vegetation. Taking into account different simulations and additional sensitivity studies with regard to spectral stability requirements, radiometric requirements and an

incorrect atmospheric correction [9], the following recommendations can be given for these bands: An optimized band B4 in the red part of the spectrum should be placed in the region 655 nm to 685 nm. Optimized bands B5 and B6 should correspond to those recommended by ESA (698 nm–713 nm and 733 nm–748 nm). The centering and width of all bands in the NIR plateau (B7, B8 and B8a) are influenced by suitable SNR requirements and limiting water vapor bands. Bands B7 and B8a should be placed in the 775- to 805-nm and 845- to 885-nm windows, respectively, providing a small margin of 5 nm on both edges to avoid the influences of water vapor and chlorophyll-a absorption. Band B7 covers a relative maximum of Fe-absorptions (soils) that might be useful in this context, but there is no need for it if the SWIR band centered at 2.2 microns is included for processing and evaluation, as iron minerals display an increasing reflectance across the entire SWIR range and thus provide the necessary spectral contrast to the absorptions in the VNIR range. Decreasing the bandwidths for B7 and B8a is not recommended because it would cause decreasing SNR with no actual benefits. The same is true for B8, reaching from 775 nm to 890 nm, which provides an optimum SNR but is slightly influenced by water vapor in its center. All three bands in the IR plateau are more or less exchangeable and fully usable for IGRM and vegetation indices approaches. A comparison of the recommended spectral design with bands of the VENµS (Vegetation and Environment monitoring on a New Micro-Satellite) sensor shows that they are in good accordance with the only significant difference in the width of B7. This is an important result as it confirms our approach and findings by an independent study.

The SWIR range is covered by two bands. The location of B11 is recommended to extend from 1550 nm to 1650 nm, and that for B12 from 2150 nm to 2250 nm. The cut-off at 2280 nm for B12 hinders the detection of Mg-OH bearing minerals and typical absorptions due to C-O bonds displayed by soils and rocks containing varieties of carbonates that take place at around 2280 nm to 2350 nm. However, this band is most useful to detect phyllosilicates, such as clays and micas, in the 2200-nm range. This is of great importance for characterizing soils in vegetation studies and can also be used for analyzing mining waste and alteration zones in exploration studies.

In the next generation of optical Sentinel sensors, the number of channels should be increased by up to 4 more desirable bands. A yellow band (620 nm) similar to the Venµs and MERIS sensor would greatly improve the quantification of phytopigments such as phycocyanin (contained in blue-green algae) within case-2 waters. It has also the potential to improve the detection of vegetation diseases such as chlorosis or the estimation of ripeness from arable crops [9]. Another band should be placed at 2.1 µm, enabling the differentiation between dry vegetation and soils via the characteristic absorption of cellulose. The urgency of this issue is driven by the fact that one third of the world's population is living in sub-humid, semi-arid or arid to hyper-arid regions covering 41% of the Earth's land mass. Monitoring the state of vitality of plants in affected areas and the borders of larger deserts are of high importance. Unfortunately, there is a strong contamination of CO_2 bands at exactly the same wavelength position, and the absorption feature can only be captured using a narrow-band design. The third band should enable the identification of Mg-OH bearing minerals and typical absorptions due to C-O bonds displayed by soils and rocks containing varieties of carbonates that take place at around 2.28 µm to 2.35 µm.

Acknowledgement

References and Notes

1. A. Börner, L. Wiest, P. Keller, R. Reulke, R. Richter, M. Schaepman, and D. Schläpfer, "SENSOR: a tool for the simulation of hyperspectral remote sensing systems," ISPRS Journal of Photogrammetry and Remote Sensing 2001, **55**, 299–312 (2001).
2. J. P. Kerekes, J. E. Baum, "Full-spectrum spectral imaging system analytical model", IEEE Transactions on Geoscience and Remote Sensing, **43**, 571–580 (2005).
3. W. Verhoef, H. Bach, "Simulation of hyperspectral and directional radiance images using coupled biophysical and atmospheric radiative transfer models," Remote Sensing of Environment, **87**, 23–41 (2003).
4. L. Guanter, K. Segl, H. Kaufmann, "Simulation of optical remote sensing scenes with application to the EnMAP hyperspectral mission," IEEE Transactions on Geoscience and Remote Sensing, **47**, 2340–2351 (2009).
5. K. Segl, L. Guanter, H. Kaufmann, "Simulation of Spatial Sensor Characteristics in the Context of the EnMAP Hyperspectral Mission," IEEE Transactions on Geoscience and Remote Sensing, **48**, 3046-3054 (2010).
6. H. Kaufmann, D. Meißner, J. Bodechtel, F.-J. Behr, "Design of spectral and panchromatic bands for the German MOMS-02 sensor," Photogrammetric Engineering and Remote Sensing, **55**, 875-881(1989).
7. M. Berger, H. Kaufmann, H., "MOMS-02 - D2/STS-55 Mission - Validation of Spectral and Panchromatic Modules," Geo-Informationssysteme, **8/2**, 21-31 (1995).
8. ESA Sentinel-2 Team, "GMES Sentinel-2 Mission Requirements Document EOP-SM/1163/MR-dr." http://www.esa.int/esaLP/SEMM4T4KXMF_LPgmes_0.html (2007).
9. K. Segl, H. Kaufmann, R. Richter, "Study for the consolidation of the Sentinel-2 spectral, radiometric and spatial resolution requirements", ESA contract 19962/06/NL/E 2006**.**
10. R. Richter,"Sentinel-2 MSI – Level 2A Products Algorithm Theoretical Basis Document" – Volume B (ATCOR) 2010, ESA contract 21450/08/I-EC.
11. A. Berk, L. S. Bernstein, G. P. Anderson, P. K. Acharya, D. C. Robertson, J. J. Chetwynd, S. M. Adler-Golden, "MODTRAN cloud and multiple scattering upgrades with application to AVIRIS," Remote Sens. Environm**, 65**, 367-375 (1998).
12. A. Berk, G. P. Anderson, P. K. Acharya, M. Hoke, J. H. Chetwynd, L. S. Bernstein, E. P. Shettle, M. W. Matthew, S. M. Adler-Golden, "MODTRAN4 Version 3 revision 1 User's Manual", Air Force Research Lab. (2003), Hanscom AFB, MA.
13. C. Schueler, L. Woody, "Digital electro-optical imaging sensors," Journal of Imaging Systems Technology, **4**, 170-200 (1992).

14. Y. J. Kaufman, A. E. Wald, L. A. Remer, B.-C. Gao, R.-R. Li, L. Flynn, "The MODIS 2.1 μm channel – correlation with visible reflectance for use in remote sensing of aerosol," IEEE TGRS, **35**, 1286-1298 (1997).

15. S. Liang, H. Fallah-Adl, S. Kalluri, J. Jaja, Y. J. Kaufman, J. R. G. Townshend, "An operational atmospheric correction algorithm for Landsat Thematic Mapper imagery over the land", J. Geophys. Res., **102**, D14, 17,173-17,186 (1997).

16. R. Santer, D. Ramon, J. Vidot, E. Dilligeard, "A surface reflectance model for aerosol remote sensing over land," Int. J. Remote Sensing, **28**, 737-760 (2007).

17. Y. J. Kaufman, D. Tanre, "Atmospherically resistant vegetation index (ARVI) for EOS-MODIS," IEEE TGRS, **30**, 261-270 (1992).

18. J. L. Deuze, F. M. Breon, C. Devaux, P. Goloub, M. Herman, B. Lafrance, F. Maignan, A. Marchand, F. Nadal, G. Perry, D. Tanre, "Remote sensing of aerosols over land surfaces from POLDER-ADEOS-1 polarized measurements, " J. Geophys. Res., **106**, 4913-4926 (2001).

19. Y. J. Kaufman, C. Sendra, "Algorithm for automatic atmospheric corrections to visible and near-IR satellite imagery," Int. J. Remote Sensing, **9**, 1357-1381 (1988).

20. R. Frouin, P. Y. Deschamp, P. Lecomte, P. "Determination from space of atmospheric total water vapor amounts by differential absorption near 940 nm : theory and airborne verification," J. Appl. Meteorol., **29**, 448-460 (1990).

21. V. Carrere, J. E. Conel, "Recovery of atmospheric water vapor total column abundance from imaging spectrometer data around 940 nm – Sensitivity analysis and applications to Airborne Visible/Infrared Imaging Spectrometer (AVIRIS) Data," Remote Sens. Environm., **44**, 179-204 (1993).

22. D. Schläpfer, C. C. Borel, J. Keller, K. I. Itten, "Atmospheric precorrected differential absorption technique to retrieve columnar water vapor," Remote Sens. Environm., **65**, 353-366 (1998).

23. B.-C. Gao, A. F. H. Goetz, "Wiscombe, W. J. Cirrus cloud detection from airborne imaging spectrometer data using the 1.38 μm water vapor band," Geophys. Res. Lett., **20**, 301-304 (1993).

24. B.-C. Gao, P. Yang, W. Han, R.-R. Li, W. J. Wiscombe, "An algorithm using visible and 1.38 μm channels to retrieve cirrus cloud reflectances from aircraft and satellite data," IEEE TGRS, **40**, 1659-1668 (2002).

25. F. Boochs, G. Kufer, G. Docker, W. Kuhbauch, "Shape of the red edge as vitality indicator for plants," International Journal of Remote Sensing **11**, 1741-1753 (1990).

26. J. R. Miller, Wu Jiyou, M.G. Boyer, M. Belanger, E. W. Hare, "Seasonal patterns in leaf reflectance red edge characteristics," International Journal of Remote Sensing **12,** 1509-1523 (1991).

27. D. N. H. Horler, J. Barber, J. P. Darch, D. C. Ferns, A. R. Barringer, "Approaches to detection of geochemical stress in vegetation," Advanced Space Research **3**, 175-179 (1983).

28. J. G. P. W. Clevers, C. Buker, "Feasibility of the red edge index for the detection of nitrogen deficiency," Proceedings of the Fifth International Colloquium, Physical Measurements and Signatures in Remote Sensing, 14-18 January, Courchevel, 165-168 (1991).

29. N. K. Patel, C. Patnaik, S. Dutta, A. M. Shekh, A. J. Dave, "Study of crop growth parameters using airborne imaging spectrometer data," International Journal of Remote Sensing **22/12**, 2401-2411 (2002).

30. S. Jacquemoud, W. Verhoef, F. Baret, C. Bacour, P. J. Zarco-Tejada, G. P. Asner, C. François, S. L. Ustin, "PROSPECT + SAIL models: a review of use for vegetation characterization," Remote Sensing of Environment **113**, 56-66 (2009).

31. J. B. Féret, C. François, G. P. Asner, A. A. Gitelson, R. E. Martin, L. P. R. Bidel, S. L. Ustin, G. le Maire, S. Jacquemoud, "PROSPECT-4 and 5: Advances in the leaf optical properties model separating photosynthetic pigments," Remote Sensing of Environment **112**, 3030-3043 (2008).

32. S. Jacquemoud, S. L. Ustin, J. Verdebout, G. Schmuck, G. Andreoli, B. Hosgood, "Estimating leaf biochemistry using the PROSPECT leaf optical properties model," Remote Sensing of Environment **56**, 194-202 (1996).

33. W. Verhoef, "Light scattering by leaf layers with application to canopy reflectance modeling: the SAIL model," Remote Sensing of Environment, **16**, 125-141 (1984)

34. J. R. Miller, E. W. Hare, J. Wu, "Quantitative characterization of vegetation red edge reflectance: an inverted-Gaussian reflectance model," International Journal of Remote Sensing **2**, 1744-1773 (1990).

35. J. R. Miller, W. Jiyou, M. G. Boyer, M. Belanger, E. W. Hare, "Seasonal patterns in leaf reflectance red edge characteristics," International Journal of Remote Sensing **12**, 1509-1523 (1991).

36. P. Ceccato, N. Gobron, S. Flasse, B. Pinty, S. Tarantola, "Designing a spectral index to estimate vegetation water content from remote sensing data: Part 1 Theoretical approach," Remote Sensing of Environment **82**, 188-197 (2002).